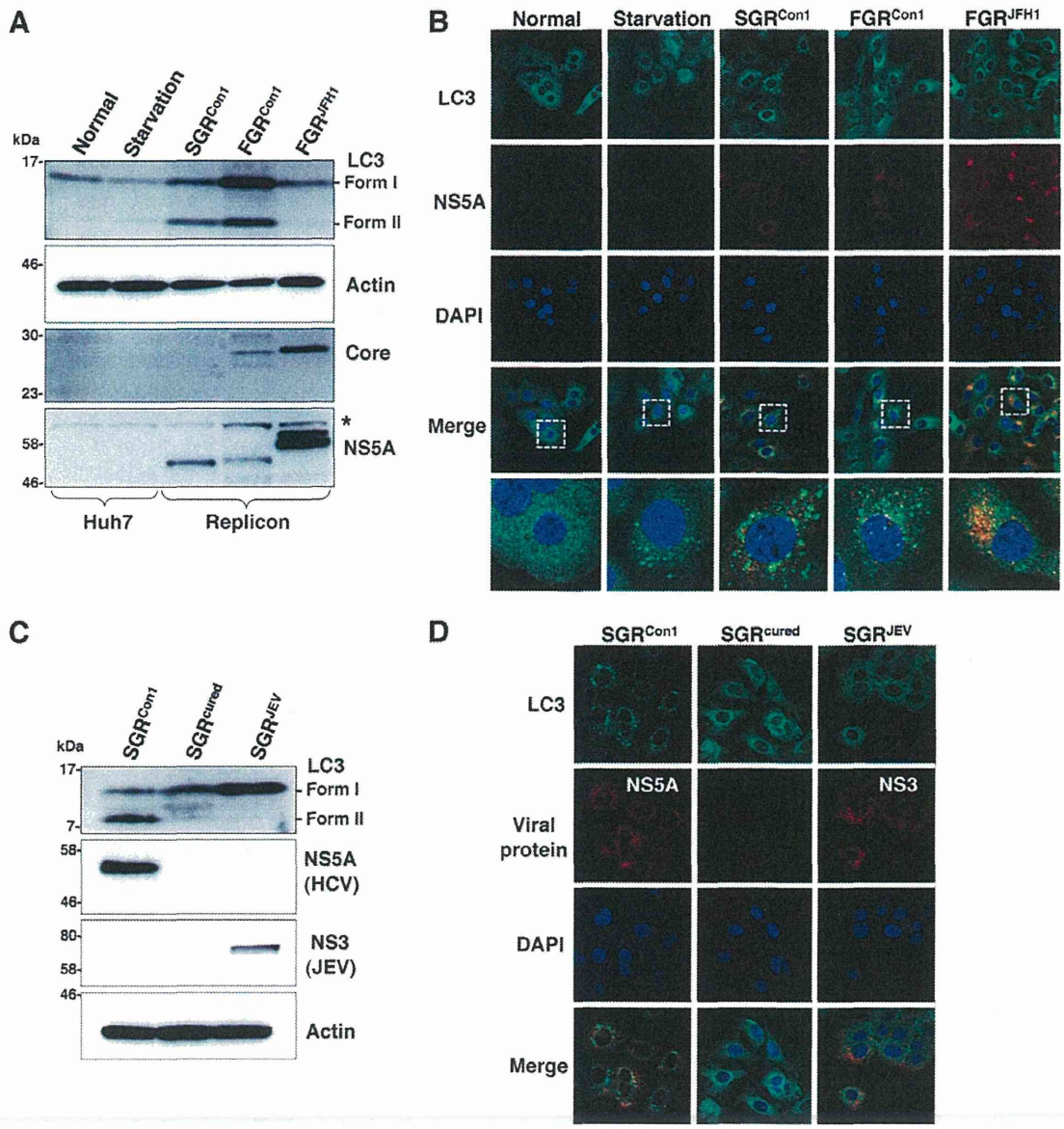

FIG. 1. Induction of autophagy in the HCV replicon cells. (A) The starved Huh7 cells and HCV replicon cells harboring a sub- or full genomic RNA of strain Con1 or strain JFH1 were subjected to immunoblotting using the appropriate antibodies. The asterisk indicates a nonspecific band. (B) Subcellular localizations of LC3 and NS5A were determined by confocal microscopy. The replicon cells and the starved Huh7 cells were stained with DAPI and then reacted with rabbit polyclonal anti-LC3 and mouse monoclonal anti-NS5A antibodies, respectively, followed by Alexa Fluor 488- and 594-conjugated secondary antibodies, respectively. The boxed areas in the merged images are magnified. (C) SGR^{Con1} cells were treated with alpha interferon for 1 week to remove the HCV replicon RNA. The resulting cells were designated SGR^{cured} cells. The SGR^{Con1}, SGR^{cured}, and SGR^{JEV} cells were lysed and subjected to immunoblotting using the appropriate antibodies. (D) Subcellular localization of LC3 and JEV NS3 and HCV NS5A was determined by confocal microscopy after staining with DAPI, followed by staining with rabbit polyclonal anti-LC3 and anti-JEV NS3 antibodies and mouse monoclonal anti-NS5A antibodies and then with the appropriate secondary antibodies. The data shown are representative of three independent experiments.

cells by treatment with the inhibitors, whereas only a slight increase was observed in the SGR^{Con1} cells (5.4-fold versus 1.6-fold) (Fig. 2A), suggesting that autophagy is suppressed in the HCV replicon cells. Furthermore, cytoplasmic accumulation of LC3 was significantly increased in the naïve Huh7 cells by treatment with the inhibitors, in contrast to the only slight increase induced by treatment in the SGR^{Con1} cells (Fig. 2B). In SGR^{Con1} cells, the LC3 foci were colocalized with the polyubiquitin-binding protein p62/SQSTM1, a specific substrate for autophagy (18), suggesting that most of the autophagosomes were distributed in the cytoplasm of the SGR^{Con1} cells (Fig. 2B and C). Next, to examine the autophagy flux in the SGR^{Con1} cells, we monitored the green fluorescent protein (GFP)-conjugated LC3 dynamics in living cells by using time-lapse imaging techniques (see movies in the supplemental material). A large number of small GFP-LC3 foci were detected in the

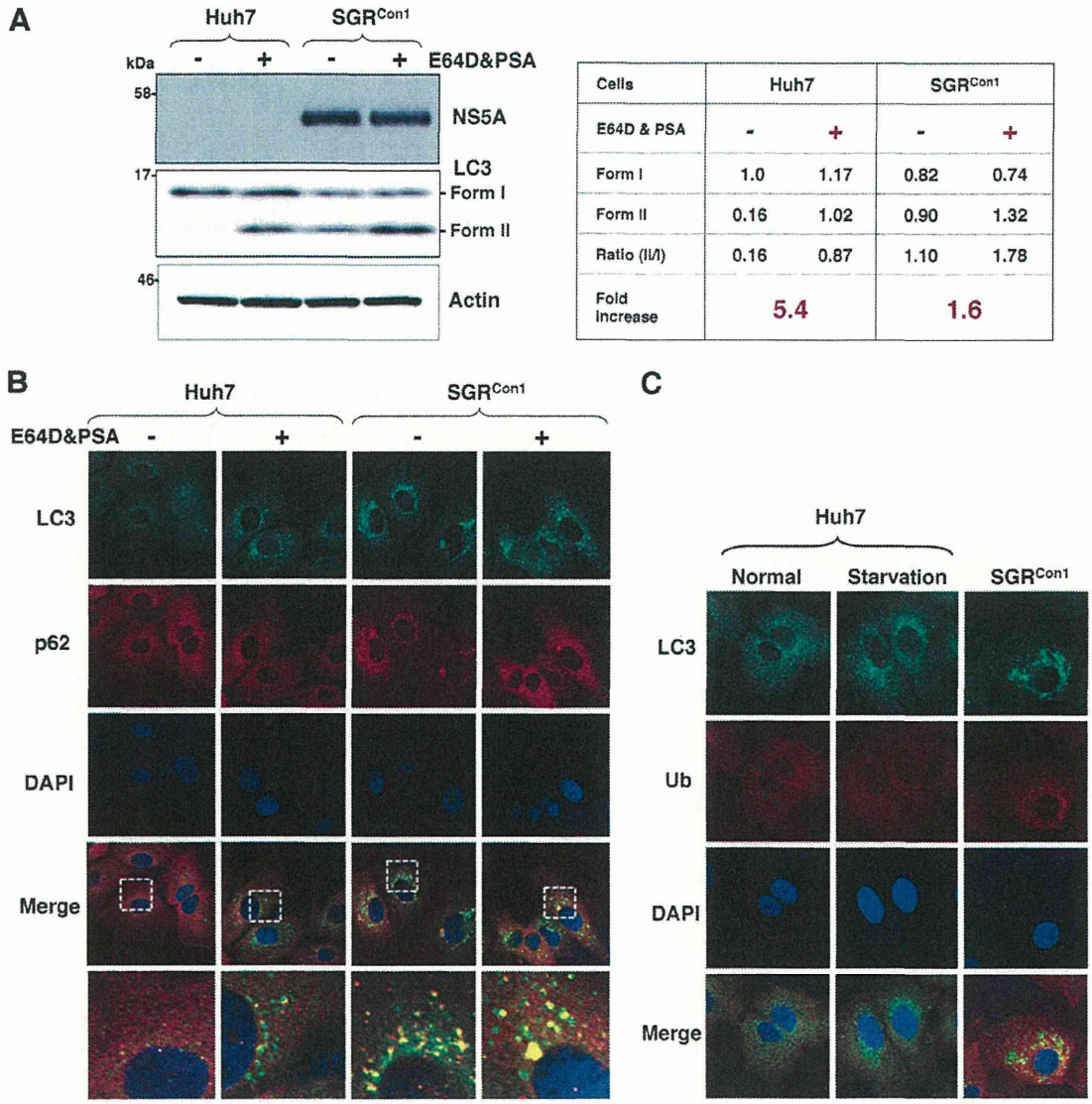

Cells	Huh7		SGR^{Con1}	
E64D & PSA	-	+	-	+
Form I	1.0	1.17	0.82	0.74
Form II	0.16	1.02	0.90	1.32
Ratio (II/I)	0.16	0.87	1.10	1.78
Fold increase	5.4		1.6	

FIG. 2. Autophagy flux is impaired in the HCV replicon cells. Autophagy flux assay using lysosomal protease inhibitors. (A) Huh7 and SGR^{Con1} cells were treated with 20 μM E64D and pepstatin A (PSA) for 6 h, and the cell lysates were subjected to immunoblotting. The density of the protein band was estimated by Multi Gauge version 2.2 (Fujifilm). (B) After nuclear staining with DAPI, the intracellular localizations of LC3 and p62 in each cell were determined by staining with rabbit polyclonal anti-LC3 and mouse monoclonal anti-62 antibodies, respectively, followed by staining with Alexa Fluor 488- and 594-conjugated secondary antibodies, respectively. The resulting cells were observed by confocal microscopy. (C) Colocalization of accumulated LC3 with ubiquitinated proteins (Ub) in SGR^{Con1} cells. Nontreated and starved Huh7 cells and SGR^{Con1} cells were fixed and stained with DAPI and rabbit anti-LC3 and anti-ubiquitin (6C1.17) (BD) polyclonal antibodies, respectively, and then with the appropriate secondary antibodies. Subcellular localizations of LC3 and Ub were determined by confocal microscopy. The data shown are representative of three independent experiments.

starved Huh7 cell, moved quickly, and finally disappeared within 30 min. Although small foci of GFP-LC3 exhibited characteristics similar to those in the starved cells, some large foci exhibited confined movement and maintained constant fluorescence for at least 3 h in the SGR^{Con1} cells. The GFP-LC3 foci in the SGR^{JFH1} cells showed characteristics similar to those in the starved cells. These results support the notion that autophagy flux is suppressed in the SGR^{Con1} cells at some step after autophagosome formation.

Impairment of autolysosomal acidification causes incomplete autophagy in the replicon cell of strain Con1. Recent studies have shown that some viruses inhibit the autophagy pathway by blocking the autolysosome formation (10, 42). Therefore, we determined the autolysosome formation in the HCV replicon cells through the fusion of autophagosome with lysosome. Colocalization of small foci of LC3 with LAMP1, a lysosome marker, was observed in the starved Huh7 cells, SGR^{Con1} cells, and SGR^{JFH1} cells but not in the SGR^{cured} cells (Fig. 3A), suggesting that autolysosomes are formed in the HCV replicon cells of both Con1 and JFH1 strains. The autolysosome is acidified by the vacuolar-type H^+ ATPase (V-ATPase) and degrades substrates by the lysosomal acidic hy-

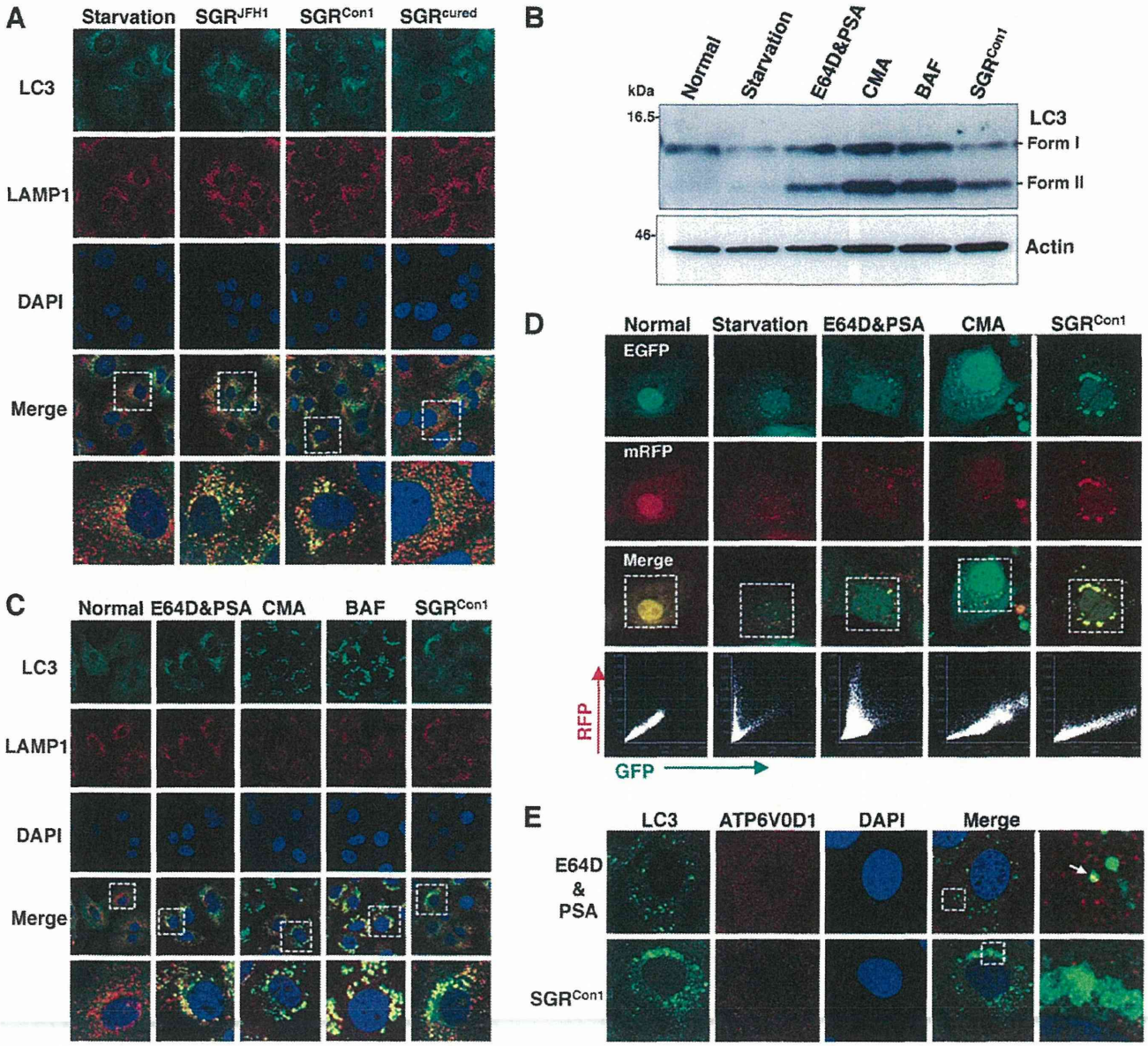

FIG. 3. Inhibition of autophagy maturation in HCV replicon cells. (A) After nuclear staining with DAPI, starved Huh7 cells, replicon cells, and SGR^{cured} cells were stained with rabbit polyclonal anti-LC3 and mouse monoclonal anti-LAMP1 antibodies followed by Alexa Fluor 488- and 594-conjugated secondary antibodies, respectively, and examined by confocal microscopy. The boxed regions in the merged images are magnified. (B and C) Huh7 cells were treated with 20 μM protease inhibitors (E64D and PSA) or a 20 nM concentration of a V-ATPase inhibitor (CMA or BAF) for 6 h. (B) Cell lysates were subjected to immunoblotting using antibodies against LC3 and β-actin. (C) Intracellular localization of LAMP1 and LC3 was determined by confocal microscopy after staining with DAPI and appropriate antibodies. The boxed areas in the merged images are magnified. (D) Tandem fluorescence-tagged LC3 assay. The expression plasmid encoding mRFP-GFP-tandem-tagged LC3 was transfected into naïve and starved Huh7 cells or into the SGR^{Con1} cells treated with the indicated inhibitors at 36 h posttransfection. The resulting cells were fixed at 42 h posttransfection, and the relative GFP and RFP signals were determined by confocal microscopy. The fluorescent values in the boxes of the merged images were determined and shown as dot plots in the bottom column of the grid, in which the *x* and *y* axes indicate the signals of GFP and RFP, respectively. (E) Huh7 cells treated with E64D and PSA and the SGR^{Con1} cells were stained with DAPI and then with rabbit polyclonal anti-LC3 and mouse monoclonal anti-ATP6V0D1 antibodies followed by Alexa Fluor 488- and 594-conjugated secondary antibodies, respectively. The boxed regions in the merged images are magnified. A white arrow indicates colocalization of LC3 and ATP6V0D1. The data shown are representative of three independent experiments.

drolases in the vesicle (2). Next, to determine the possibility of a deficiency in the acidification of the autolysosome on the autophagic dysfunction in the Con1 replicon cells, Huh7 cells were treated with the protease inhibitors E64D and pepstatin A (PSA) or with each of the V-ATPase inhibitors concanamycin A (CMA) and bafilomycin A1 (BAF). The amount of LC3-II was significantly increased in Huh7 cells treated with the inhibitors just as in the SGR^{Con1} cells (Fig. 3B). Further-

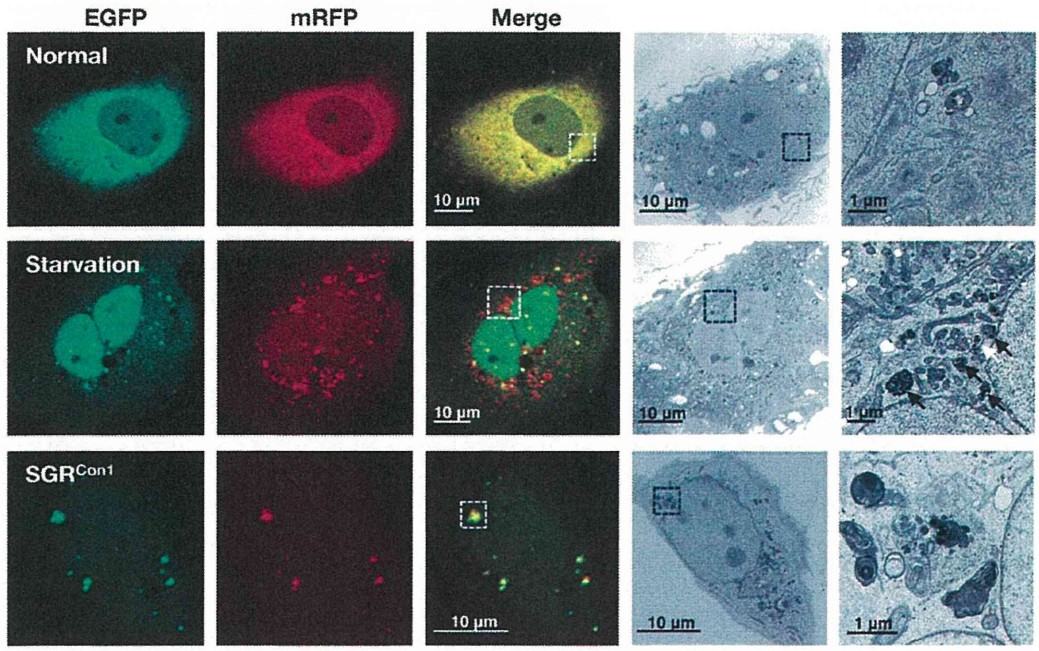

FIG. 4. Correlative fluorescence microscopy-electron microscopy (FM-EM) analysis. The expression plasmid encoding mRFP-GFP-tandem-tagged LC3 was transfected into naïve and starved Huh7 cells or into the SGR^{Con1} cells as described in the legend to Fig. 3D, and the mRFP-GFP-tandem-tagged LC3 signals were observed at 36 h posttransfection. The boxed regions in the merged images are magnified. The data shown are representative of three independent experiments.

more, the large foci of LC3 colocalized with LAMP1 appeared in the cells treated with the V-ATPase inhibitors, as seen in SGR^{Con1} cells (Fig. 3C). These results suggest that stacked autophagosome flux caused by the inhibition of lysosomal degradation or acidification exhibits characteristics similar to those observed in the Con1 replicon cells.

Since the fluorescence of GFP but not that of monomeric red fluorescent protein (mRFP) disappears under the acidic environment, expression of mRFP-GFP tandem fluorescent-tagged LC3 (tfLC3) is capable of being used to monitor the acidic status of the autolysosome (24). Both GFP and mRFP fluorescent signals were unfused, some of them accumulated as small foci in Huh7 cells after starvation or by treatment with the protease inhibitors, and half of the foci of mRFP were not colocalized with those of GFP (Fig. 3D), indicating that half of the foci are in an acidic state due to maturation into an autolysosome after fusion with a lysosome. On the other hand, the large foci of GFP and mRFP were completely colocalized in Huh7 cells treated with CMA or in the SGR^{Con1} cells. These results suggest that the large foci of LC3 in the SGR^{Con1} cells are not under acidic conditions. Recently, it was shown that the lack of lysosomal acidification in human genetic disorders due to dysfunction in assembly/sorting of V-ATPase induces incomplete autophagy similar to that observed in SGR^{Con1} cells (31, 45). Therefore, to explore the reason for the lack of acidification of the autolysosome in the SGR^{Con1} cells, we examined the subcellular localization of ATP6V0D1, a subunit of the integral membrane V_0 complex of V-ATPase. Colocalization of ATP6V0D1 with large foci of LC3 was observed in Huh7 cells treated with the protease inhibitors but not in SGR^{Con1} cells (Fig. 3E), suggesting that dislocation of V-ATPase may participate in the impairment of the autolysosomal acidification in the SGR^{Con1} cells.

We further examined the morphological characteristics of the LC3-positive compartments by using correlative fluorescence microscopy-electron microscopy (FM-EM) (Fig. 4). The starved Huh7 cells exhibited a small double-membrane vesicle (white arrow) and high-density single-membrane structures (black arrows) in close proximity to the correlative position of the GFP- and mRFP-positive LC3 compartments, which are considered to be the autophagosome and lysosome/autolysosome, respectively. In contrast, many high-density membranous structures were detected in the correlative position of the large GFP- and mRFP-positive LC3 compartment in the SGR^{Con1} cells, which is well consistent with the observation in the time-lapse imaging in which small foci of LC3 headed toward and assembled with the large LC3-positive compartment (see movies in the supplemental material). These results suggest that the formation of large aggregates with aberrant inner structures in the SGR^{Con1} cells may impair maturation of the autolysosome through the interference of further fusion with functional lysosomes for the degradation.

The secretion of immature cathepsin B is enhanced in the replicon cell of strain Con1. Lysosomal acidification is required for the cleavage of cathepsins for activation, and cathepsin B (CTSB) is processed under acidic conditions (13). Although a marginal decrease of CTSB was detected in the whole lysates of the SGR^{Con1} cells, a significant reduction in the expression of both unprocessed (pro-CTSB) and matured CTSB was observed in the lysosomal fractions of the SGR^{Con1} cells compared with those of the naïve Huh7 and the SGR^{cured} cells (Fig. 5A). LAMP1 was concentrated at a similar level in

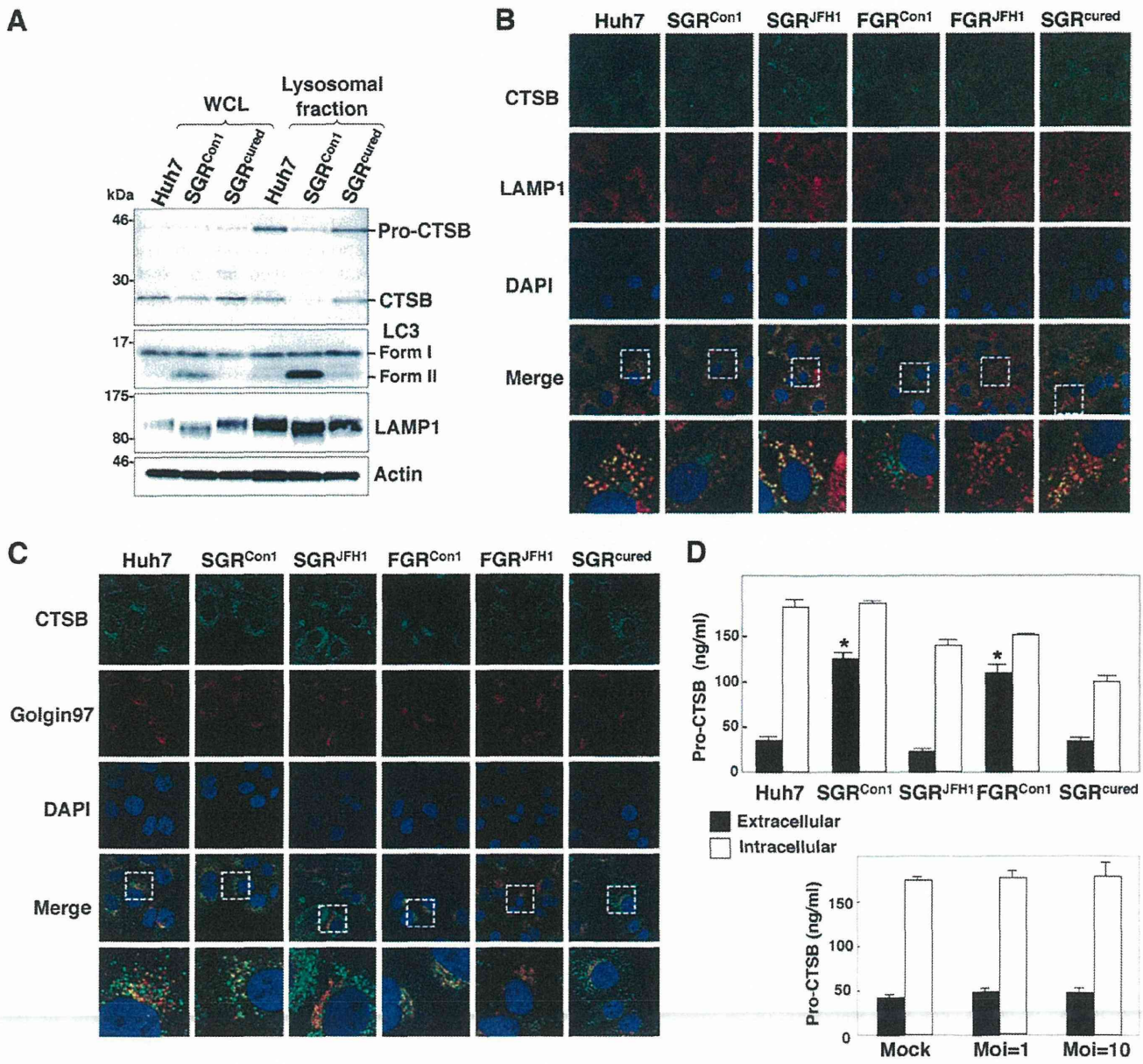

FIG. 5. Enhanced secretion of pro-CTSB in the HCV replicon cells. (A) The whole-cell lysate (WCL) and lysosomal fraction prepared from Huh7, SGR^{Con1}, and SGR^{cured} cells were subjected to immunoblotting. (B and C) Huh7 cells, HCV replicon cells, and SGR^{cured} cells were stained with DAPI, rabbit polyclonal anti-CTSB antibody, and mouse anti-LAMP1 (B) or anti-Golgin97 (C) antibody. The boxed areas in the merged images are magnified. (D) Expression of pro-cathepsin B in the culture supernatants (black bars) and cell lysates (white bars) of the Huh7, SGR^{Con1}, SGR^{JFH1}, FGR^{Con1}, and SGR^{cured} cells and the SGR^{cured} cells infected with HCVcc at a multiplicity of infection (Moi) of 1 or 10 and incubated for 72 h was determined by enzyme-linked immunosorbent assay (ELISA). The error bars indicate standard deviations. The asterisks indicate significant differences ($P < 0.01$) versus the control value. The data shown are representative of three independent experiments.

the lysosomal fractions of the cells, whereas LC-II was detected in the fractions of the SGR^{Con1} cells but not in those of Huh7 and the SGR^{cured} cells, suggesting that autophagosomes and/or autolysosomes in the SGR^{Con1} cells are fractionated in the lysosomal fraction. Colocalization of CTSB with LAMP1 was observed in the naïve Huh7 cells, in the SGR^{cured} cells, and in the replicon cells harboring a sub- or a full genomic RNA of strain JFH1 (SGR^{JFH1} and FGR^{JFH1}, respectively) but not in those of strain Con1 (SGR^{Con1} and FGR^{Con1}) (Fig. 5B). On the other hand, CTSB was colocalized with Golgin97, a marker for the Golgi apparatus, in the SGR^{Con1} and FGR^{Con1} cells but not in other cells (Fig. 5C). Since previous reports suggested that the alkalization in the lysosome triggers secretion of the unprocessed lysosomal enzymes (19, 41), we next determined the secretion of pro-CTSB in the replicon cells. Secretion of the pro-CTSB was significantly enhanced in the replicon cells of strain Con1 but not in those of strain JFH1 and naïve and cured cells (Fig. 5D, top). Furthermore, secretion of pro-CTSB

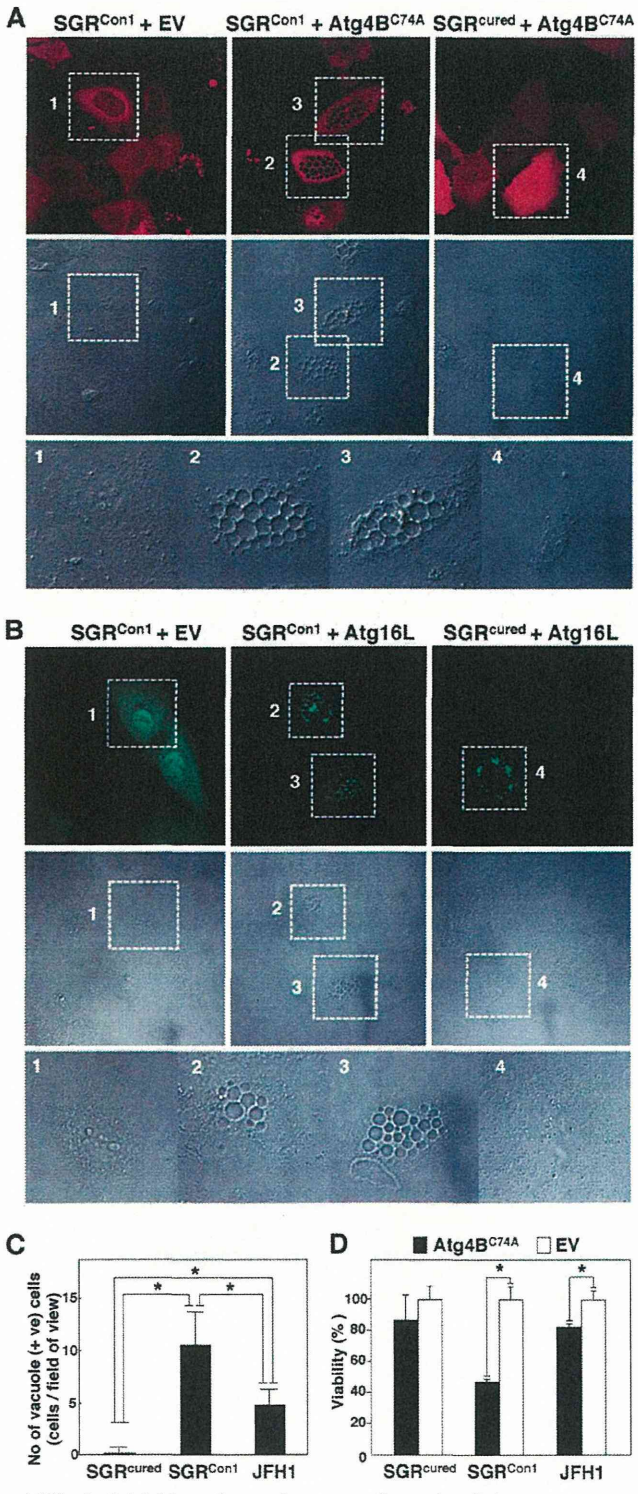

FIG. 6. Inhibition of autophagosome formation induces severe cytoplasmic vacuolations leading to cell death in the HCV replicon cells. (A) SGR^{Con1} and SGR^{cured} cells transfected with pStrawberry-$Atg4B^{C74A}$ or empty vector pStrawberry (EV) were fixed at 48 h posttransfection and examined by fluorescence microscopy. The boxed areas in the phase-contrast images are magnified. (B) SGR^{Con1} and SGR^{cured} cells transfected with pEGFP-Atg16L or EV were examined by fluorescence microscopy at 48 h posttransfection. The boxed areas in the phase-contrast images are magnified. (C) SGR^{cured}, SGR^{Con1}, and SGR^{cured} cells infected with JFH1 virus were transfected with pStrawberry-$Atg4B^{C74A}$, and the number of vacuole-positive cells in each of nine fields of view was counted at 48 h posttransfection. (D) SGR^{cured}, SGR^{Con1}, and SGR^{cured} cells infected with JFH1 virus were transfected with pStrawberry-$Atg4B^{C74A}$ (black bars) or EV (white bars), and cell viability was determined at 6 days posttransfection by using CellTiter-Glo (Promega) according to the manufacturer's protocol. The asterisks indicate significant differences ($P < 0.05$) versus the control value. The data shown are representative of three independent experiments.

was not observed in the cured cells infected with HCVcc, an infectious HCV strain derived from strain JFH1 (Fig. 5D, bottom). Collectively, these results suggest that the dysfunction of lysosomal acidification contributes to the impairment of autophagy in the HCV replicon cells of strain Con1.

Autophagy induced in cells replicating HCV is required for cell survival. Finally, we examined the pathological significance of autophagy during HCV replication. Atg4B is known as an LC3-processing protease, and overexpression of its protease-inactive mutant ($Atg4B^{C74A}$) results in inhibition of the autophagosome formation (7). To our surprise, severe cytoplasmic vacuolation was observed in the SGR^{Con1} cells expressing $Atg4B^{C74A}$ (Fig. 6A). These vacuolations were also observed in the SGR^{Con1} cells by the expression of Atg16L (Fig. 6B), a molecule that is an essential component of the autophagy complex and that, if expressed in excess amounts, can disrupt the autophagosome formation (8). Expression of $Atg4B^{C74A}$ induced a higher level of vacuole formation in the Con1 replicon cells than in cells infected with JFH1 virus but not in the cured cells (Fig. 6C). Along with these vacuolations, cell viability was significantly decreased by the expression of $Atg4B^{C74A}$ in SGR^{Con1} cells and slightly in JFH1 virus-infected cells (Fig. 6D). These results suggest that autophagy induced by the RNA replication of HCV is required for host cell survival.

DISCUSSION

In the present study, we demonstrated that two genotypes of HCV induce autophagy, whereas intact autophagy flux is required for the host cell to survive. The cell death characterized by cytoplasmic vacuolation that was induced in the HCV replicon cells by the inhibition of the autophagosome formation is similar to type III programmed cell death, which is distinguishable from apoptosis and autophagic cell death (4). Type III programmed cell death has been observed in the neurodegenerative diseases caused by the deposit of cytotoxic protein aggregates (15).

We previously reported that HCV hijacks chaperone complexes, which regulates quality control of proteins into the membranous web for circumventing unfolded protein response during efficient genome replication (53); in other words, the replication of HCV exacerbates the generation of proteins associated with cytotoxicity. In the experiments using a chimpanzee model, HCV of genotype 1 was successfully used to reproduce acute and chronic hepatitis similar to that in the human patients (3, 57), and transgenic mice expressing viral proteins of HCV of genotype 1b have been shown to develop

Sjögren syndrome, insulin resistance, hepatic steatosis, and hepatocellular carcinoma (27, 28). In contrast, HCVcc, based on the genotype 2a strain JFH1 isolated from a patient with fulminant hepatitis C (33, 56), was unable to establish chronic infection in chimpanzees (56) or to induce cell damage and inflammation in chimeric mice xenotransplanted with human hepatocytes (17). These results imply that the onset of HCV pathogenesis could be dependent not only upon an amount but also on a property of deposited proteins, and they might explain the aggravated vacuolations under the inhibition of autophagosome formation in strain Con1 compared to that in strain JFH1. Interestingly, the overexpression of $Atg4B^{C74A}$ or Atg16L causes eccentric cell death in the Con1 replicon cells in which autophagy flux is already disturbed. Thus, we speculated that the quarantine of undefined abnormalities endowed with high cytotoxicity by the engulfing of the autophagic membrane might be sufficient for the amelioration of HCV-induced degeneration. The autophagosomal dysfunction observed in the Con1 replicon cells may suggest that a replicant of strain Con1 was more sensitive to the lysosomal vacuolation than that of strain JFH1. Because a limitation of our study was that we were unable to use infectious HCV of other strains, it is still unclear whether the autophagic degradation can be impaired only in the replicon of HCV strain Con1 or genotype 1.

We also demonstrated that HCV replication of strain Con1 but not that of strain JFH1 facilitates the secretion of pro-CTSB. It has been well established that the secretion of pro-CTSB is enhanced in several types of tumors (26, 50). The secretion of CTSB, like the secretion of matrix metalloproteases, is a marker of the progression of the proteolytic degradation of the extracellular matrix, which plays an important part in cancer invasion and metastasis. Since infection with HCV of genotype 1 is clinically considered a risk factor for the development of hepatocellular carcinoma (14, 51), the enhanced secretion of pro-CTSB by the replication of genotype 1 strains might synergistically promote infiltration of hepatocellular carcinoma.

As shown elsewhere (see movies in the supplemental material), although most degradations of the autophagosome were impaired due to a dislocalization of a V-ATPase subunit, some autophagic degradation was achieved in the SGR^{Con1} cells similar to that in the starved Huh7 cells. Moreover, the stagnated autophagy flux was rescued by the treatment of alpha interferon accompanied by elimination of HCV (Fig. 1C and D). Interestingly, we observed neither a significant impairment of lysosomal degradation nor the intracellular activity of cathepsins in the replicon cells of HCV strain Con1 (data not shown). Therefore, there might be a specific dysfunction within the autolysosome during the replication of HCV strain Con1. Detailed studies are needed to elucidate how HCV strain Con1 disturbs the sorting of V-ATPase.

A close relationship between autophagy and the immune system has been gradually unveiled (47). Autophagy assists not only in the direct elimination of pathogens by hydrolytic degradation but also in antigen processing in antigen-presenting cells such as macrophage and dendritic cells (DC) for presentation by major histocompatibility complex (MHC) I and II (11). Moreover, autophagy plays important roles in T lymphocyte homeostasis (44). As such, in some instances, interruptions of autophagy can allow microorganisms to escape from the host immune system. Indeed, the immune response against herpes simplex virus was suppressed by blocking the autophagy (6). With regard to HCV, functionally impaired DC dysfunctions marked by poor DC maturation, impaired antigen presentation, and attenuated cytokine production have been reported in tissue culture models and chronic hepatitis C patients (1, 22, 46). In addition, reduction of cell surface expression of MHC-I in HCV genotype 1b replicon cells has been reported (55). We confirmed that levels of cell surface expression of MHC-I in the replicon cells of genotype 1b, but not of genotype 2a, were reduced in comparison with those in the cured cells (data not shown). Hence it might be feasible to speculate that the replication of HCV RNA of genotype 1 induces an incomplete autophagy for attenuating antigen presentation to establish persistent infection. In contrast, autophagy is known to serve as a negative regulator of innate immunity (21, 54). A recent report demonstrated that autophagy induced by infection with strain JFH1 or dengue virus attenuates innate immunity to promote viral replication (23), indicating that an HCV genotype 2a strain may facilitate autophagy to evade innate immunity.

In this study, we demonstrated that HCV utilizes autophagy to circumvent the cell death induced by vacuole formation for its survival. This unique strategy of HCV propagation may provide new clues to the virus-host interaction and, ultimately, to the pathogenesis of infection by various genotypes of HCV.

ACKNOWLEDGMENTS

We thank H. Murase and M. Tomiyama for their secretarial work. We also thank R. Bartenschlager and T. Wakita for providing cell lines and plasmids.

This work was supported in part by grants-in-aid from the Ministry of Health, Labor, and Welfare (Research on Hepatitis), the Ministry of Education, Culture, Sports, Science, and Technology, and the Osaka University Global Center of Excellence Program.

REFERENCES

1. **Auffermann-Gretzinger, S., E. B. Keeffe, and S. Levy.** 2001. Impaired dendritic cell maturation in patients with chronic, but not resolved, hepatitis C virus infection. Blood **97**:3171–3176.
2. **Beyenbach, K. W., and H. Wieczorek.** 2006. The V-type H+ ATPase: molecular structure and function, physiological roles and regulation. J. Exp. Biol. **209**:577–589.
3. **Bradley, D. W.** 2000. Studies of non-A, non-B hepatitis and characterization of the hepatitis C virus in chimpanzees. Curr. Top. Microbiol. Immunol. **242**:1–23.
4. **Clarke, P. G.** 1990. Developmental cell death: morphological diversity and multiple mechanisms. Anat. Embryol. (Berl.) **181**:195–213.
5. **Dreux, M., P. Gastaminza, S. F. Wieland, and F. V. Chisari.** 2009. The autophagy machinery is required to initiate hepatitis C virus replication. Proc. Natl. Acad. Sci. U. S. A. **106**:14046–14051.
6. **English, L., et al.** 2009. Autophagy enhances the presentation of endogenous viral antigens on MHC class I molecules during HSV-1 infection. Nat. Immunol. **10**:480–487.
7. **Fujita, N., et al.** 2008. An Atg4B mutant hampers the lipidation of LC3 paralogues and causes defects in autophagosome closure. Mol. Biol. Cell **19**:4651–4659.
8. **Fujita, N., et al.** 2008. The Atg16L complex specifies the site of LC3 lipidation for membrane biogenesis in autophagy. Mol. Biol. Cell **19**:2092–2100.
9. **Fujitani, Y., C. Ebato, T. Uchida, R. Kawamori, and H. Watada.** 2009. β-cell autophagy: a novel mechanism regulating β-cell function and mass: lessons from β-cell-specific Atg7-deficient mice. Islets **1**:151–153.
10. **Gannage, M., et al.** 2009. Matrix protein 2 of influenza A virus blocks autophagosome fusion with lysosomes. Cell Host Microbe **6**:367–380.
11. **Gannage, M., and C. Munz.** 2009. Autophagy in MHC class II presentation of endogenous antigens. Curr. Top. Microbiol. Immunol. **335**:123–140.
12. **Hara, T., et al.** 2006. Suppression of basal autophagy in neural cells causes neurodegenerative disease in mice. Nature **441**:885–889.
13. **Hasilik, A.** 1992. The early and late processing of lysosomal enzymes: proteolysis and compartmentation. Experientia **48**:130–151.

14. **Hatzakis, A., et al.** 1996. Hepatitis C virus 1b is the dominant genotype in HCV-related carcinogenesis: a case-control study. Int. J. Cancer **68:**51–53.
15. **Hirabayashi, M., et al.** 2001. VCP/p97 in abnormal protein aggregates, cytoplasmic vacuoles, and cell death, phenotypes relevant to neurodegeneration. Cell Death Differ. **8:**977–984.
16. **Hiraga, N., et al.** 2011. Rapid emergence of telaprevir resistant hepatitis C virus strain from wildtype clone in vivo. Hepatology (Baltimore, Md.) **54:** 781–788.
17. **Hiraga, N., et al.** 2007. Infection of human hepatocyte chimeric mouse with genetically engineered hepatitis C virus and its susceptibility to interferon. FEBS Lett. **581:**1983–1987.
18. **Ichimura, Y., E. Kominami, K. Tanaka, and M. Komatsu.** 2008. Selective turnover of p62/A170/SQSTM1 by autophagy. Autophagy **4:**1063–1066.
19. **Isidoro, C., et al.** 1995. Altered intracellular processing and enhanced secretion of procathepsin D in a highly deviated rat hepatoma. Int. J. Cancer **60:**61–64.
20. **Jacobson, I. M., P. Cacoub, L. Dal Maso, S. A. Harrison, and Z. M. Younossi.** 2010. Manifestations of chronic hepatitis C virus infection beyond the liver. Clin. Gastroenterol. Hepatol. **8:**1017–1029.
21. **Jounai, N., et al.** 2007. The Atg5 Atg12 conjugate associates with innate antiviral immune responses. Proc. Natl. Acad. Sci. U. S. A. **104:**14050–14055.
22. **Kanto, T., et al.** 1999. Impaired allostimulatory capacity of peripheral blood dendritic cells recovered from hepatitis C virus-infected individuals. J. Immunol. **162:**5584–5591.
23. **Ke, P. Y., and S. S. Chen.** 2011. Activation of the unfolded protein response and autophagy after hepatitis C virus infection suppresses innate antiviral immunity in vitro. J. Clin. Invest. **121:**37–56.
24. **Kimura, S., N. Fujita, T. Noda, and T. Yoshimori.** 2009. Monitoring autophagy in mammalian cultured cells through the dynamics of LC3. Methods Enzymol. **452:**1–12.
25. **Kiyosawa, K., et al.** 1990. Interrelationship of blood transfusion, non-A, non-B hepatitis and hepatocellular carcinoma: analysis by detection of antibody to hepatitis C virus. Hepatology **12:**671–675.
26. **Koblinski, J. E., et al.** 2002. Interaction of human breast fibroblasts with collagen I increases secretion of procathepsin B. J. Biol. Chem. **277:**32220–32227.
27. **Koike, K., et al.** 1997. Sialadenitis histologically resembling Sjogren syndrome in mice transgenic for hepatitis C virus envelope genes. Proc. Natl. Acad. Sci. U. S. A. **94:**233–236.
28. **Koike, K., T. Tsutsumi, H. Yotsuyanagi, and K. Moriya.** 2010. Lipid metabolism and liver disease in hepatitis C viral infection. Oncology **78**(Suppl. 1)**:**24–30.
29. **Komatsu, M., et al.** 2006. Loss of autophagy in the central nervous system causes neurodegeneration in mice. Nature **441:**880–884.
30. **Komatsu, M., et al.** 2007. Homeostatic levels of p62 control cytoplasmic inclusion body formation in autophagy-deficient mice. Cell **131:**1149–1163.
31. **Lee, J. H., et al.** 2010. Lysosomal proteolysis and autophagy require presenilin 1 and are disrupted by Alzheimer-related PS1 mutations. Cell **141:** 1146–1158.
32. **Levine, B., and G. Kroemer.** 2008. Autophagy in the pathogenesis of disease. Cell **132:**27–42.
33. **Lindenbach, B. D., et al.** 2005. Complete replication of hepatitis C virus in cell culture. Science **309:**623–626.
34. **Lohmann, V., et al.** 1999. Replication of subgenomic hepatitis C virus RNAs in a hepatoma cell line. Science **285:**110–113.
35. **Manns, M. P., et al.** 2001. Peginterferon alfa-2b plus ribavirin compared with interferon alfa-2b plus ribavirin for initial treatment of chronic hepatitis C: a randomised trial. Lancet **358:**958–965.
36. **McHutchison, J. G., et al.** 2009. Telaprevir with peginterferon and ribavirin for chronic HCV genotype 1 infection. N. Engl. J. Med. **360:**1827–1838.
37. **Mizushima, N.** 2007. Autophagy: process and function. Genes Dev. **21:**2861–2873.
38. **Moradpour, D., F. Penin, and C. M. Rice.** 2007. Replication of hepatitis C virus. Nat. Rev. Microbiol. **5:**453–463.
39. **Moriishi, K., and Y. Matsuura.** 2007. Host factors involved in the replication of hepatitis C virus. Rev. Med. Virol. **17:**343–354.
40. **Moriishi, K., and Y. Matsuura.** 2003. Mechanisms of hepatitis C virus infection. Antivir. Chem. Chemother. **14:**285–297.
41. **Oda, K., Y. Nishimura, Y. Ikehara, and K. Kato.** 1991. Bafilomycin A1 inhibits the targeting of lysosomal acid hydrolases in cultured hepatocytes. Biochem. Biophys. Res. Commun. **178:**369–377.
42. **Orvedahl, A., et al.** 2007. HSV-1 ICP34.5 confers neurovirulence by targeting the Beclin 1 autophagy protein. Cell Host Microbe **1:**23–35.
43. **Poordad, F., et al.** 2011. Boceprevir for untreated chronic HCV genotype 1 infection. N. Engl. J. Med. **364:**1195–1206.
44. **Pua, H. H., I. Dzhagalov, M. Chuck, N. Mizushima, and Y. W. He.** 2007. A critical role for the autophagy gene Atg5 in T cell survival and proliferation. J. Exp. Med. **204:**25–31.
45. **Ramachandran, N., et al.** 2009. VMA21 deficiency causes an autophagic myopathy by compromising V-ATPase activity and lysosomal acidification. Cell **137:**235–246.
46. **Saito, K., et al.** 2008. Hepatitis C virus inhibits cell surface expression of HLA-DR, prevents dendritic cell maturation, and induces interleukin-10 production. J. Virol. **82:**3320–3328.
47. **Schmid, D., and C. Munz.** 2007. Innate and adaptive immunity through autophagy. Immunity **27:**11–21.
48. **Schutte, K., J. Bornschein, and P. Malfertheiner.** 2009. Hepatocellular carcinoma—epidemiological trends and risk factors. Dig. Dis. **27:**80–92.
49. **Sir, D., et al.** 2008. Induction of incomplete autophagic response by hepatitis C virus via the unfolded protein response. Hepatology **48:**1054–1061.
50. **Sloane, B. F., et al.** 2005. Cathepsin B and tumor proteolysis: contribution of the tumor microenvironment. Semin. Cancer Biol. **15:**149–157.
51. **Stankovic-Djordjevic, D., et al.** 2007. Hepatitis C virus genotypes and the development of hepatocellular carcinoma. J. Dig. Dis. **8:**42–47.
52. **Strader, D. B., T. Wright, D. L. Thomas, and L. B. Seeff.** 2004. Diagnosis, management, and treatment of hepatitis C. Hepatology **39:**1147–1171.
53. **Taguwa, S., et al.** 2009. Cochaperone activity of human butyrate-induced transcript 1 facilitates hepatitis C virus replication through an Hsp90-dependent pathway. J. Virol. **83:**10427–10436.
54. **Tal, M. C., et al.** 2009. Absence of autophagy results in reactive oxygen species-dependent amplification of RLR signaling. Proc. Natl. Acad. Sci. U. S. A. **106:**2770–2775.
55. **Tardif, K. D., and A. Siddiqui.** 2003. Cell surface expression of major histocompatibility complex class I molecules is reduced in hepatitis C virus subgenomic replicon-expressing cells. J. Virol. **77:**11644–11650.
56. **Wakita, T., et al.** 2005. Production of infectious hepatitis C virus in tissue culture from a cloned viral genome. Nat. Med. **11:**791–796.
57. **Walker, C. M.** 1997. Comparative features of hepatitis C virus infection in humans and chimpanzees. Springer Semin. Immunopathol. **19:**85–98.
58. **Wasley, A., and M. J. Alter.** 2000. Epidemiology of hepatitis C: geographic differences and temporal trends. Semin. Liver Dis. **20:**1–16.
59. **Wong, J., et al.** 2008. Autophagosome supports coxsackievirus B3 replication in host cells. J. Virol. **82:**9143–9153.
60. **Yoshimori, T., and T. Noda.** 2008. Toward unraveling membrane biogenesis in mammalian autophagy. Curr. Opin. Cell Biol. **20:**401–407.

JOURNAL OF VIROLOGY, Nov. 2011, p. 10976–10988 Vol. 85, No. 21
0022-538X/11/$12.00 doi:10.1128/JVI.00846-11

Heterogeneous Nuclear Ribonucleoprotein A2 Participates in the Replication of Japanese Encephalitis Virus through an Interaction with Viral Proteins and RNA▽

Hiroshi Katoh,[1] Yoshio Mori,[3] Hiroto Kambara,[1] Takayuki Abe,[1] Takasuke Fukuhara,[1] Eiji Morita,[1] Kohji Moriishi,[4] Wataru Kamitani,[2] and Yoshiharu Matsuura[1]*

Department of Molecular Virology[1] and Global COE Program,[2] Research Institute for Microbial Diseases, Osaka University, Osaka, Department of Virology III, National Institute of Infectious Diseases, Tokyo,[3] and Department of Microbiology, Faculty of Medicine, Yamanashi University, Yamanashi,[4] Japan

Received 26 April 2011/Accepted 9 August 2011

Japanese encephalitis virus (JEV) is a mosquito-borne flavivirus that is kept in a zoonotic transmission cycle between pigs and mosquitoes. JEV causes infection of the central nervous system with a high mortality rate in dead-end hosts, including humans. Many studies have suggested that the flavivirus core protein is not only a component of nucleocapsids but also an important pathogenic determinant. In this study, we identified heterogeneous nuclear ribonucleoprotein A2 (hnRNP A2) as a binding partner of the JEV core protein by pulldown purification and mass spectrometry. Reciprocal coimmunoprecipitation analyses in transfected and infected cells confirmed a specific interaction between the JEV core protein and hnRNP A2. Expression of the JEV core protein induced cytoplasmic retention of hnRNP A2 in JEV subgenomic replicon cells. Small interfering RNA (siRNA)-mediated knockdown of hnRNP A2 resulted in a 90% reduction of viral RNA replication in cells infected with JEV, and the reduction was cancelled by the expression of an siRNA-resistant hnRNP A2 mutant. In addition to the core protein, hnRNP A2 also associated with JEV nonstructural protein 5, which has both methyltransferase and RNA-dependent RNA polymerase activities, and with the 5′-untranslated region of the negative-sense JEV RNA. During one-step growth, synthesis of both positive- and negative-strand JEV RNAs was delayed by the knockdown of hnRNP A2. These results suggest that hnRNP A2 plays an important role in the replication of JEV RNA through the interaction with viral proteins and RNA.

Japanese encephalitis virus (JEV) belongs to the genus *Flavivirus* within the family *Flaviviridae*. Members of the genus *Flavivirus* are predominantly arthropod-borne viruses, such as dengue virus (DEN), West Nile virus (WNV), yellow fever virus (YFV), and tick-borne encephalitis virus, and frequently cause significant morbidity and mortality in mammals and birds (46). JEV is distributed in the south and southeast regions of Asia and is kept in a zoonotic transmission cycle between pigs or birds and mosquitoes (46, 69). JEV spreads to dead-end hosts, including humans, through the bite of JEV-infected mosquitoes and causes infection of the central nervous system, with a high mortality rate (46). JEV has a single-stranded positive-strand RNA genome of approximately 11 kb, which is capped at the 5′ end but lacks modification of the 3′ terminus by polyadenylation (38). The genomic RNA carries a single large open reading frame, and a polyprotein translated from the genome is cleaved co- and posttranslationally by host and viral proteases to yield three structural proteins—the core, precursor membrane, and envelope protein—and seven nonstructural (NS) proteins—NS1, NS2A, NS2B, NS3, NS4A, NS4B, and NS5 (61).

The core protein of flaviviruses has RNA-binding activity through basic amino acid clusters located in both the amino and carboxyl termini, indicating that the core protein forms a nucleocapsid interacting with viral RNA (23). In spite of the replication of flaviviruses in the cytoplasm, the core protein is also detected in the nucleus, especially the nucleolus, suggesting that the core protein plays an additional role in the life cycle of flaviviruses (6, 42, 48, 66). We previously reported that a mutant JEV defective in the nuclear localization of the core protein had impaired growth in mammalian cells and impaired neuroinvasiveness in mice (48) and that the nuclear and cytoplasmic localization of the JEV core protein is dependent on binding to the host nucleolar protein B23 (62). In addition to the JEV core protein, other flavivirus core proteins bind to several host proteins, such as Jab (a component of the COP9 signalosome complex) (53), the chaperone protein Hsp70 (54), heterogeneous nuclear ribonucleoprotein (hnRNP) K (7), and the apoptotic proteins HDM2 (71) and Daxx (50), and regulate their functions. In the cytoplasm, the core protein of flaviviruses was found at the sites of viral RNA replication (40, 68). A recent report demonstrated a coupling between viral RNA synthesis and RNA encapsidation (21, 55, 61). Therefore, the flavivirus core protein plays crucial roles not only in the viral life cycle, including RNA replication and assembly, but also in viral pathogenesis.

Replication of flaviviruses is initiated by a viral RNA replication complex through a process of RNA-dependent RNA polymerization on the endoplasmic reticulum (ER) membranes. The intracellular membrane rearrangements that are induced by the *Flaviviridae* family are best characterized for Kunjin virus (KUN), which is the Australian variant of WNV

* Corresponding author. Mailing address: Department of Molecular Virology, Research Institute for Microbial Diseases, Osaka University, 3-1 Yamada-oka, Suita, Osaka 565-0871, Japan. Phone: 81-6-6879-8340. Fax: 81-6-6879-8269. E-mail: matsuura@biken.osaka-u.ac.jp.

▽ Published ahead of print on 24 August 2011.

(14). KUN induces two distinct membrane structures: large clusters of double-membrane vesicles (DMV) and a second membrane structure that consists of convoluted membranes (CM). It has been demonstrated that DMV are the sites of viral replication, whereas CM are the sites of viral polyprotein processing (67). Clusters of DMV have also been observed in other flaviviruses (65). The NS3 and NS5 proteins have been identified as the major components of the viral RNA replication complex (4). NS5, the largest and most conserved flavivirus protein, contains sequences homologous to those of methyltransferase (MTase) and RNA-dependent RNA polymerase (RdRp), which are responsible for methylation of the 5′ cap structure (9, 27) and for viral RNA replication (1, 12, 74), respectively. In addition, NS5 inhibits the interferon-stimulated Jak-Stat signaling pathway through the activation of protein tyrosine phosphatases during JEV infection (37).

In this study, we identified hnRNP A2 as a binding partner of the JEV core protein by pulldown purification and mass spectrometry. hnRNP A2 and B1, which are the most abundant of the approximately 20 major hnRNPs, are produced by alternative splicing from a single gene and differ from each other by only a 12-amino-acid insertion in the N-terminal region of A2 (28). hnRNP A2 participates in posttranscriptional regulation in both the nucleus and cytoplasm and also is involved in telomere biogenesis. hnRNP A2 was translocated from the nucleus to the cytoplasm upon infection with JEV and facilitated viral replication through interaction with the JEV core and NS5 proteins and with the 5′-untranslated region (UTR) of the negative-strand JEV RNA, suggesting an important role for hnRNP A2 in the life cycle of JEV.

MATERIALS AND METHODS

Cells. Vero (African green monkey kidney), 293T (human kidney), and Huh7 (human hepatocellular carcinoma) cells were maintained in Dulbecco's modified Eagle's minimal essential medium (DMEM) supplemented with 100 U/ml penicillin, 100 μg/ml streptomycin, nonessential amino acids (Sigma, St. Louis, MO), and 10% fetal bovine serum (FBS). JEV subgenomic replicon (SGR) cells were generated as described previously (18). Briefly, Huh7 and 293T cells were electroporated with *in vitro*-transcribed RNA from pJErepIRESpuro, and drug-resistant clones were selected by treatment with puromycin (Invivogen, San Diego, CA) at a final concentration of 1 μg/ml. The resulting replicon cells were designated JEV-SGR-Huh7 and JEV-SGR-293T cells, respectively. Cell viability was determined by using CellTiter-Glo (Promega, Madison, WI) according to the manufacturer's instructions.

Plasmids. Plasmids encoding hemagglutinin (HA)-, FLAG-, and MEF (consisting of a myc tag, the tobacco etch virus protease cleavage site, and a FLAG tag)-tagged JEV core (pCAGPM-Core-HA, pCAGPM-FLAG-Core, and pCAGPM-MEF-Core, respectively) were prepared as described previously (49, 62). Plasmids encoding HA-tagged JEV NS proteins (pCAGPM-HA-NS) were generated by previously described methods (18). The cDNA of human hnRNP A2 was amplified by PCR and cloned into pcDNA 3.1 containing a FLAG tag gene (pcDNA 3.1 N-FLAG) (62), pCAGPM containing an HA tag gene (pCAGPM N-HA) (48), and pGEX 4T-1 (GE Healthcare, Buckinghamshire, United Kingdom) for expression in bacteria as a glutathione *S*-transferase (GST) fusion protein. The resulting plasmids were designated pcDNA-FLAG-hnRNP A2, pCAGPM-HA-hnRNP A2, and pGEX-hnRNP A2, respectively. A series of deletion mutants of the core protein, NS5, and hnRNP A2 was synthesized by PCR-based mutagenesis using a KOD-Plus mutagenesis kit (Toyobo, Osaka, Japan). A silent mutant of HA-hnRNP A2 (siR) and a mutant of FLAG-tagged core with Gly^{42} and Pro^{43} replaced by Ala (FLAG-CoreM) were also generated by PCR-based mutagenesis. All plasmids were confirmed by sequencing with an ABI Prism 3130 genetic analyzer (Applied Biosystems, Tokyo, Japan).

Antibodies. Anti-JEV core rabbit polyclonal antibody (PAb) was prepared as described previously (48). Anti-JEV NS3 mouse monoclonal antibody (MAb) was prepared by using a recombinant protein spanning amino acids (aa) 171 to 619 of JEV NS3. Anti-JEV NS5 mouse MAb was generated with recombinant NS5 at Bio Matrix Research Inc. (Chiba, Japan). Anti-FLAG mouse MAb (M2), anti-hnRNP A2/B1 mouse MAb (DP3B3), anti-β-actin mouse MAb, and anti-FLAG rabbit PAb were purchased from Sigma. Anti-nucleoporin p62 mouse MAb and anti-GM130 mouse MAb were purchased from BD Biosciences (Franklin Lakes, NJ). Anti-JEV envelope protein mouse MAb (6B4A-10), anti-HA mouse MAb (HA11), anti-PA28α rabbit PAb, anti-calregulin rabbit PAb (H-170), and anti-HA rat MAb (3F10) were purchased from Chemicon (Temecula, CA), Covance (Richmond, CA), Affinity Bioreagents (Golden, CO), Santa Cruz (California, CA), and Roche (Mannheim, Germany), respectively.

MEF purification. pCAGPM-MEF-Core was transfected into 293T cells and subjected to MEF purification as described previously (17, 62). Proteins interacting with the JEV core protein were separated by 12.5% sodium dodecyl sulfate-polyacrylamide gel electrophoresis (SDS-PAGE) and visualized by silver staining. The stained bands were excised, digested in gels with Lys-C, and analyzed by direct nanoflow liquid chromatography-tandem mass spectrometry (LC-MS/MS) (17).

Transfection, immunoprecipitation, and immunoblotting. Plasmids were transfected into 293T cells by use of TransIT LT1 (Mirus, Madison, WI), and cells were harvested at 24 h posttransfection and subjected to immunoprecipitation and immunoblotting as described previously (15). The immunoprecipitates were boiled in loading buffer and subjected to 12.5% or 15% SDS-PAGE. The proteins were transferred to polyvinylidene difluoride membranes (Millipore, Bedford, MA) and incubated with the appropriate antibodies. The immune complexes were visualized with SuperSignal West Femto substrate (Thermo Scientific, Rockford, IL) and detected by use of an LAS-3000 image analyzer system (Fujifilm, Tokyo, Japan).

Immunofluorescence microscopy and subcellular fractionation. Vero cells infected with JEV at a multiplicity of infection (MOI) of 1.0 or JEV-SGR-Huh7 cells transfected with pCAGPM-FLAG-Core and/or pCAGPM-HA-hnRNP A2 were fixed with cold acetone, incubated with appropriate antibodies, and examined by use of a Fluoview FV1000 laser scanning confocal microscope (Olympus, Tokyo, Japan) at 24 h postinfection/posttransfection. The subcellular localization of the proteins was determined by fractionation using a nuclear/cytosol fractionation kit (Biovision, Mountain, CA) according to the manufacturer's instructions.

Gene silencing. The small interfering RNAs (siRNAs) si-A2#1 (5′-GGAUU AUUUAAUAACAUU-3′) and si-A2#2 (5′-GGAGAGUAGUUGAGCCAA A-3′) (47) were used for knockdown of endogenous hnRNA A2/B1. The negative control, siCONTROL nontargeting siRNA-2 (si-NC), which exhibits no downregulation of any human genes, was purchased from Dharmacon (Buckinghamshire, United Kingdom). JEV-SGR-293T and naïve 293T cells grown on 6-, 12-, and 24-well plates were transfected with 30, 12, and 6 nM siRNA, respectively, by use of Lipofectamine RNAiMax (Invitrogen, Carlsbad, CA).

Real-time PCR. Total RNA was prepared from cells by use of an RNeasy minikit (Qiagen, Tokyo, Japan), and first-strand cDNA was synthesized using a ReverTra Ace qPCR RT kit (Toyobo). The level of each cDNA was determined by using Platinum SYBR green qPCR SuperMix UDG (Invitrogen), and fluorescent signals were analyzed by use of an ABI Prism 7000 system (Applied Biosystems). Strand-specific reverse transcription (RT) was performed using the following primers: 5′-ATGAGGCTGCCACACCAGAT-3′ for positive-strand JEV RNA, 5′-TACTCCGACGGTGTGGTCTA-3′ for negative-strand JEV RNA, and an oligo(dT) primer for β-actin mRNA. The JEV NS5 and β-actin genes were amplified using the following primer pairs: 5′-GCCGGGTGGGAC ACTAGAAT-3′ and 5′-TGGACAGCGATGTTCGTGAA-5′ for NS5 and 5′-A CGGGGTCACCCACACTGTGC-3′ and 5′-CTAGAAGCATTTGCGGTGGA CGATG-3′ for β-actin. The value of JEV RNA was normalized to that of β-actin mRNA.

Virus titration. Virus infectivity was determined by an immunostaining focus assay with Vero cells and was expressed in focus-forming units (FFU). Briefly, viruses were serially diluted and inoculated onto monolayers of Vero cells. After 1 h of absorption, cells were washed with serum-free DMEM and cultured in DMEM containing 5% FBS and 1.25% methylcellulose 4000. At 48 h postinfection, cells were fixed with 4% paraformaldehyde and permeabilized with 0.5% Triton X-100, and infectious foci were stained with anti-JEV envelope protein mouse MAb (6B4A-10) and visualized with a Vectastain Elite ABC anti-mouse IgG kit with VIP substrate (Vector Laboratories, Burlingame, CA).

Immunoprecipitation–RT-PCR. Cells (1×10^6) transfected with pCAGPM-HA-hnRNP A2 were infected with JEV at an MOI of 1.0 and then incubated with 400 μl of RNA-protein binding buffer (10 mM HEPES [pH 7.3], 500 mM KCl, 1 mM EDTA, 2 mM $MgCl_2$, 0.1% NP-40, yeast tRNA [0.1 μg/μl], RNase inhibitor [1 U/ml] [Toyobo], and protease inhibitor cocktail [Complete; Roche]) for 10 min at 4°C at 24 h postinfection. After centrifugation at 16,000 × *g* at 4°C for 20 min, the supernatants were incubated with 20 μl of protein G-Sepharose